Available online at www.sciencedirect.com
SCIENCE DIRECT®
Journal of Physics and Chemistry of Solids 66 (2005) 2281–2289
JOURNAL OF PHYSICS AND CHEMISTRY OF SOLIDS
www.elsevier.com/locate/jpcs

Electron–hole excitations in NiO: LSDA + U-based calculations vs. inelastic X-ray scattering and ellipsometry measurements

A.G. Eguiluz [a,b,*], O.D. Restrepo [a,b], B.C. Larson [b], J.Z. Tischler [b], P. Zschack [c], G.E. Jellison [b]

[a] *Department of Physics and Astronomy, The University of Tennessee, 1401 Circle Drive, Knoxville, TN 37996-1200, USA*
[b] *Condensed Matter Sciences Division, Oak Ridge National Laboratory, Oak Ridge, TN 37831-6030, USA*
[c] *Frederick Seitz Materials Research Laboratory, University of Illinois, Urbana-Champaign, IL 61801, USA*

Abstract

The performance of the LSDA + U functional—in particular, the quality of the ground-state—is tested via calculations of the electron–hole excitations of NiO, which are compared with (non-resonant) inelastic X-ray scattering (IXS) and ellipsometry measurements. The dynamical density-response calculations are performed within the random-phase approximation (RPA), defining an LSDA + U/RPA density-response method. A significant success of this method is the insight it provides into the main loss present in the IXS data above the NiO optical gap, namely, a peak lying at ~7.5 eV. This excitation, which is shown to be collective in nature, and to be induced by e_g–e_g transitions, provides a direct link between the correlated e_g-states and the IXS data. This finding illustrates the power of IXS, combined with correlated-band-structure theory (here, LSDA + U theory), for the investigation of the electronic structure of strongly correlated materials. At the same time, our results indicate that the LSDA + U/RPA response method does not represent a complete theory.
© 2005 Elsevier Ltd. All rights reserved.

The Hohenberg–Kohn–Sham density-functional theory (DFT) [1,2] provides the most successful framework available today for the evaluation of the ground state density—and, thus, of 'everything else' pertaining to the ground state of an interacting many-electron system—from first-principles. Key to the enormous impact of DFT on condensed-matter physics is the remarkable (a posteriori) numerical accuracy of the simplest, non-trivial, approximation for the exchange-correlation energy functional, namely, the local-density approximation (LDA) [3].

Now, it is well known that the LDA (or its spin-polarized version, the LSDA) fails qualitatively in the description of the electronic and magnetic properties of strongly correlated materials. The reason for this failure is easy to visualize. Materials such as transition metal oxides and heavy fermion systems feature ions with incomplete d or f shells, respectively; the strong atomic-like correlations, which control the physics of the electrons in these shells, are, by definition, not treated properly by the LSDA functional, as the same models the correlations in terms of a locally homogeneous electron gas—which represents the extreme opposite limit vs. the case of localized electrons in the incomplete shells.

Among several methods which have been tailored for 'going beyond' the LSDA non-perturbatively the self-interaction-correction (SIC) method [4,5] (typically implemented starting from LSDA), and the LSDA + U method [6–10], stand out. (We say 'non-perturbatively' in the sense that the treatment of atomic-like correlations recognizes at the outset the strongly inhomogeneous environment of the partially filled shells.) Here we confine our attention to the latter method, which has proved quite popular in recent years [11].

In this paper, after a brief overview of the LSDA + U method, we recall some essentials of the (formally exact) dynamical density-response method provided by time-dependent density-functional theory (TDDFT) [12,13]. This sketch of the theory helps visualize the fact that the use of LSDA + U orbitals and eigenvalues amounts to a physically motivated TDDFT-like incursion into the strong-correlation problem, and its manifestation via electron–hole excitations on an energy scale of the key 'parameter', i.e., the Hubbard U. Our approach, which relies on the use of the random-phase approximation for

* Corresponding author. Address: Department of Physics and Astronomy, The University of Tennessee, 1401 Circle Drive, Knoxville, TN 37996-1200, USA. Tel.: +1 423 974 9642; fax: +1 423 974 7843.
E-mail address: eguiluz@utk.edu (A.G. Eguiluz).

0022-3697/$ - see front matter © 2005 Elsevier Ltd. All rights reserved.
doi:10.1016/j.jpcs.2005.09.092

the electron dynamics, defining what we refer to as LSDA + U/RPA method, is good enough to provide insight into the most intriguing feature of the IXS data for energy transfers above the NiO 'optical' gap. At the same time, our results highlight the limitations of the LSDA + U/RPA method.

We stress at the outset that in our comparison of theory with experiment, we will not be suggesting that we may determine 'the' value of U which may be appropriate for the q-dependent electron–hole excitation process; we will argue that such procedure (which has been adopted by other authors in related work [14]) is, in general, 'risky,' without a proper inclusion of the U in the dynamics.

1. Theoretical essentials

The basic physical idea behind the LSDA + U method is to insert Hubbard-like physics on top of the LSDA. In essence, as in the Anderson model, we start out by separating electrons into two subsystems: localized d-like or f-like electrons, for which the interactions are described by a 'Hubbard U,' and delocalized s and p electrons, which can be described by LSDA.

In order to account for the Coulomb interactions between the localized electrons we introduce the model Hamiltonian

$$\hat{H} = \frac{U}{2} \sum_{m,m',\sigma} \hat{n}_{m,\sigma}\hat{n}_{m',-\sigma} + \frac{(U-J)}{2} \sum_{m\neq m',\sigma} \hat{n}_{m,\sigma}\hat{n}_{m',\sigma}. \quad (1)$$

We take it as a given that appropriate localized orbitals, characterized by quantum numbers m, σ (the latter referring to the spin projection) *can be identified*. In Eq. (1) we have denoted by $\hat{n}_{m,\sigma}$ the operators for the occupation numbers for these orbitals. The Coulomb energy U and the exchange interaction J are viewed as adjustable parameters. (The 'Hubbard U' can be calculated from first principles within LSDA using constrained DFT techniques [15]; such 'first-principles' value provides guidance as to 'reasonable' values to be used in the LSDA + U method. This point is retaken below.) The above Hamiltonian is treated via a Hartree–Fock decoupling, which is a reasonable approximation for the subspace spanned by the localized electron states, i.e., we set

$$\langle\hat{H}\rangle = \frac{U}{2} \sum_{m,m',\sigma} n_{m,\sigma}n_{m',-\sigma} + \frac{(U-J)}{2} \sum_{m\neq m',\sigma} n_{m,\sigma}n_{m',\sigma}, \quad (2)$$

where $n_{m,\sigma} = \langle\hat{n}_{m,\sigma}\rangle$ are *orbital-dependent* occupation *numbers*. The LSDA + U energy functional is then written in the form

$$E_{\mathrm{LSDA+U}} = E_{\mathrm{LSDA}} + \langle\hat{H}\rangle, \quad (3)$$

which is further augmented by adding a term (not shown here) which corrects for double-counting of the correlations already built into the LSDA; several approximate forms for this term are available [10]. (Note: Eq. (3) is not quite the full form of $E_{\mathrm{LSDA+U}}$; nonetheless, the above sketch illustrates the main ideas. For details, the reader is urged to consult Refs. [6–10].)

We emphasize that the main justification for the use of the LSDA + U functional is that we are introducing qualitatively correct many-body physics—e.g., the *suppression of charge fluctuations due to atomic-like correlations*. This is beautifully illustrated by Fig. 2 of Ref. [16]. At the same time, by construction, the occupied and empty states within the subspace of localized orbitals are shifted relative to each other, which drives the formation of the gap (this is the job performed by U). Significantly, the full complexity of the hybridization between d-like states deriving from the cation, and p-like states derived from the oxygen atoms is treated on the same footing with the above many-body effect, leading to an unbiased treatment of the charge-transfer process which sets the energy scale for the actual gap.

The LSDA + U functional has been tested successfully many times in recent years, by comparing predicted ground-state observables such as magnetic moments (see, e.g., Refs. [9,17]) vs. experiment. Such exercise represents an ab initio test of the LSDA + U functional. Frequently, the performance of the functional, and the quality of the underlying ground state, is assessed in terms of spectroscopic observables, such as photoemission line shapes. In this context, it should be noted that the eigensolutions of the LSDA + U functional are expected, on intuitive grounds, to be closer to physical quasiparticle states than is the case for Kohn–Sham states. However, the significance of the LSDA + U 'orbitals' does not follow uniquely from a well-defined many-body approximation for the electron self-energy (an effort has been made to link the LSDA + U picture to the GW approximation of many-body physics [10]).

In the present work, we use another approach for testing the LSDA + U functional (or any other functional, for that matter), i.e., by benchmarking its performance via predictions for the spectrum of *electron–hole excitations*. What is significant about this approach is that the quantity we calculate, the dynamical density-response function, is linked *exactly*, in the Born approximation, to experimental cross sections for inelastic X-ray scattering (IXS) [18], for which we present new, state-of-the-art measurements. Our approach probes in detail electronic degrees of freedom which are summed over in, for example, the magnetic moments. In addition, we have access to the full richness of the quantum-mechanical phase space for electron–hole excitations, which in conventional optical measurements are probed in a much-more restricted way; in fact, we present new ellipsometry measurements to drive this point across. Our analysis is here confined to the case of NiO, a time-honored archetype of a Mott–Hubbard (more properly, charge-transfer) antiferromagnetic insulator.

Our calculations are framed in the spirit of time-dependent density-functional theory (TDDFT) [12,13], which constitutes a formally exact generalization of DFT for the description of an interacting, many-electron system evolving in the presence of an external, *time-dependent* potential $v_{\mathrm{ext}}(\vec{x},t)$. In the linear-response regime, in TDDFT we introduce the dynamical density-response function for interacting electrons via the equation

$$\chi[n_0](\vec{x}t;\vec{x}'t') = \frac{\delta n[v_{\mathrm{ext}}](\vec{x}t)}{\delta v_{\mathrm{ext}}(\vec{x}'t')}\Big|_{v_{\mathrm{ext}}[n_0]}, \quad (4)$$

where the functional derivative is evaluated at the ground-state potential—which is one-to-one with the ground-state density n_0, according to DFT [19]; note that from this observation it follows that the *dynamical* χ is a functional of n_0 (we will in general omit explicit reference to this functional dependence of χ) [20]. TDDFT allows us to introduce a similar definition for the density-response function $\chi_s[n_0]$ for uncorrelated (Kohn–Sham) electrons (the functional derivative is now taken with respect to the potential $v_s(\vec{x},t)$ in which the Kohn–Sham electrons evolve). Invoking the elegant one-to-one mappings which are central to the TDDFT method, leads to the rigorous result (first proved by Petersilka, Gossmann and Gross [21]) that the density-response function obeys the *exact* integral equation (which we write down symbolically)

$$\chi = \chi_s + \chi_s(v + f_{xc})\chi, \tag{5}$$

where the so-called many-body kernel f_{xc}, which accounts for all dynamical correlations between electrons and holes, is defined by the equation

$$f_{xc}[n_0](\vec{x}t;\vec{x}'t') = \frac{\delta V_{xc}[n](\vec{x}t)}{\delta n(\vec{x}'t')}\Big|_{n_0}. \tag{6}$$

In this paper, we confine ourselves to a *random phase approximation* (RPA) description of the dynamics, which corresponds to ignoring the many-body kernel, i.e., we set $f_{xc} = 0$. This approximation, when combined with the use of LSDA + U ground states in the evaluation of χ_s, turns out to be quite successful, by comparison with the IXS experiments reported herein; insight as to why this is so, is provided below; at the same time, we will present clear indications as to the limitations of the method. (For recent successful implementations of this scheme for metals and oxides which do not fall in the strongly correlated category, see Refs. [22,23,24], where some details are given as to the construction of χ_s from the knowledge of the Kohn–Sham band structure and orbitals, which we evaluate within the full-potential LAPW method [25]).

The use of the LSDA + U functional raises a conceptual issue which must be addressed, namely, the Bloch eigensolutions of the LSDA + U functional are not Kohn–Sham states. Thus, strictly, we are not in a position to evaluate a Kohn–Sham response function χ_s on the basis of the LSDA + U band structure and 'orbitals.' (An implementation of the LSDA + U method via the optimized-potential method of TDDFT [26] would lead to a strict realization of the above TDDFT response theory, as the eigensolutions would then be Kohn–Sham states; this observation suggests a direction for future efforts.) In brief, the approach adopted here embodies the evaluation of a physically motivated density-response function obtained via a TDDFT-like scheme from the knowledge of the LSDA + U ground state, combined with RPA dynamics. We refer to this scheme as LSDA + U/RPA. (Our 'pragmatic' approach was actually hinted at above when we noted [20] that $\chi_s[n_0]$ is a functional of the ground-state density (this is an implicit functional dependence via the Kohn-Sham orbitals); that observation, coupled with the fact that the LSDA + U functional provides a good approximation for the ground-state density (and magnetic moment) of NiO [9,10], underlies our scheme—which admittedly relies on the assumption that the orbitals coming out of the LSDA + U ground state calculation are meaningful, in the present context.)

The theoretical framework is completed by recalling that the differential cross section for a process in which a hard X-ray undergoes a single scattering event [19], with transfer of energy $\hbar\omega$ and momentum $\hbar\vec{q}$ is given by [18]

$$\frac{d^2\sigma}{d\Omega\, d\omega} = \left(\frac{d\sigma}{d\Omega}\right)_0 S(\vec{q};\omega), \tag{7}$$

$(d\sigma/d\Omega)_0 = r_0^2(\vec{e}_i\cdot\vec{e}_f)^2\omega_f/\omega_i$ being the Thomson cross section, where r_0 is the 'classical electron radius' ($r_0 = e^2/mc^2$), and the remaining variables refer to the polarization vector and frequency of the incident ('i') and scattered ('f') photons.

In Eq. (7) we have introduced the dynamical structure factor $S(\vec{q};\omega)$, which, making use of the fluctuation–dissipation theorem, can be expressed as

$$S(\vec{q};\omega) = -2\hbar V \,\mathrm{Im}\, \chi_{\vec{G},\vec{G}}(\vec{q}-\vec{G}), \tag{8}$$

in terms of the (Fourier transform of) the density-response function χ. *Eqs. (5), (7), and (8) embody a 'first principles' approach for testing the interplay between electronic structure and IXS data.* We emphasize that this comparison involves no ad hoc assumptions, such as conjectures about the nature of the final state (often introduced in the analysis of, e.g. photoemission), or arbitrary scale factors.

Having made the previous point, it is important to expand a little on a related issue, which leads to a meaningful comparison with the IXS data—namely, this comparison is done in absolute units. In effect, we note that in Eq. (8) V is the volume of the macrocrystal on whose sides we apply periodic (Born–von Karman (BvK)) boundary conditions. Clearly, $S(\vec{q};\omega)$ is an extensive quantity. In practice, the thermodynamic limit is realized for sufficiently large BvK volumes; in that case, any residual (numerical) dependence of $S(\vec{q};\omega)$ on V is gone, and the only such dependence is via the overall factor of the BvK volume V; this can be checked [27] via calculations for denser and denser meshes—which define a new V in each case. We can then (i.e., for sufficiently dense k-meshes) define a dynamical structure factor per unit volume, by pulling the factor V from the above result, i.e.,

$$s(\vec{q};\omega) = -2\hbar \,\mathrm{Im}\, \chi_{\vec{G},\vec{G}}(\vec{q}-\vec{G}), \tag{9}$$

thereby defining a scattering cross section per unit volume,

$$\frac{1}{V}\frac{d^2\sigma}{d\Omega\, d\omega} = \left(\frac{d\sigma}{d\Omega}\right)_0 s(\vec{q};\omega). \tag{10}$$

In the results presented below, it is $s(\vec{q};\omega)$ which is evaluated from the solution of Eq. (5), and also measured via IXS (as noted shortly)—which amounts to a comparison in absolute units. This feature of our method sets the stage for an unbiased identification of physical processes.

2. Experimental

Non-resonant inelastic X-ray scattering measurements of $s(\vec{q};\omega)$ were made for momentum transfers perpendicular to <001> and <111>-oriented NiO single crystals on the UNICAT ID-33 beamline at the Advanced Photon Source (APS) at Argonne National Laboratory. The measurements were made using incident beam energies of 7.59 keV, for which the 111 Si high heat-load monochromator provided incident beam powers of $\sim 10^{12}$ Hz. Together with a spherically bent Ge <111> analyzer in near backscattering geometry, the overall energy resolution of the measurements was ~1.1 eV. The quasi-elastic scattering tails near $\Delta E = 0$ were removed using measurements made with a wide band-gap insulator. The measurements of $s(\vec{q};\omega)$ were reduced to absolute units ($\mathrm{eV}^{-1}\,\mathrm{Å}^{-3}$) using the first-moment, f-sum rule calibration of the IXS system for Al [28]. As described in detail in Ref. [28], the scale factor for measurements on NiO is obtained directly from the scale factor for Al by multiplying by the ratio of the mass absorption coefficients.

The optical functions of NiO were determined from ellipsometry measurements using a two-modulator generalized ellipsometer (2-MGE) [29] from 220 to 840 nm (5.64–1.476 eV). The surface roughness of the sample was determined by modeling the near-surface region as a Bruggeman effective medium [30] with 50% voids and 50% underlying material, and by modeling the optical functions of NiO using a Lorentz oscillator [31]. Using the determined surface roughness thickness (7.2 nm), the entire ellipsometric spectrum was used to determine the refractive index (n) and extinction coefficient (k) of NiO as described in [31].

3. Results and discussion

We start with reference to Fig. 1, which contains a key message, at the outset. The figure shows the measured $s(\vec{q};\omega)$ for a representative wave vector transfer, together with two calculations of the same quantity (Eq. (9)), obtained starting from LSDA and LSDA+U ground states, respectively, from which χ_s was evaluated, and the response χ was subsequently obtained by solving the integral Eq. (5) within RPA [32]; in the case of LSDA+U ground state, this is that we referred above as the LSDA+U/RPA method. The LSDA+U-based calculation here corresponds to the choice $U = 8$ eV, which is the value suggested by constrained-DFT calculations (implemented in LSDA) [15].

Fig. 1 highlights in a striking way the qualitative failure of the LSDA description of the electronic structure of NiO. Indeed, the LSDA-based spectrum not only displays the well-known problem of the size of the optical gap, but the whole line shape of $s(\vec{q};\omega)$ is completely off, containing spurious peaks. By contrast, the LSDA+U-based $s(\vec{q};\omega)$ works remarkably well (other than the exaggerated value of the calculated electron–hole gap), which argues in favor of the quality of the underlying LSDA+U electronic structure. This message will be emphasized further in the remainder of this presentation.

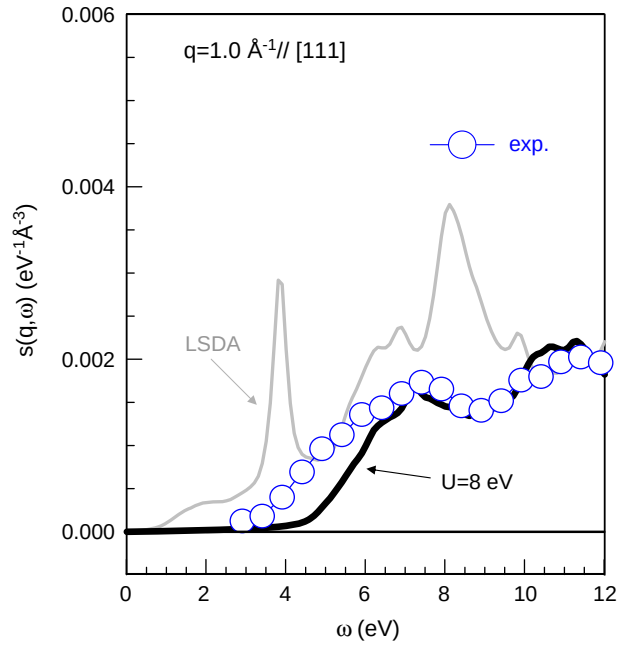

Fig. 1. Comparison of the measured $s(\vec{q};\omega)$ for NiO for $|\vec{q}| = 1.0\ \mathrm{A}^{-1}$, with $\vec{q}$ along [111], with results for the same observable calculated on the basis of LSDA and LSDA+U (for $U = 8$ eV) ground states. The comparison (as in all other figures) is in absolute units. See text for details.

Fig. 2 shows the experimental $s(\vec{q};\omega)$ covering a range of wave vector transfers along the [111] direction. It is apparent that the dominant feature above the ~4 eV optical gap is a loss lying at ~7.5 eV. Interestingly, the spectral weight of this loss depends rather markedly on wave vector transfer; in fact (not

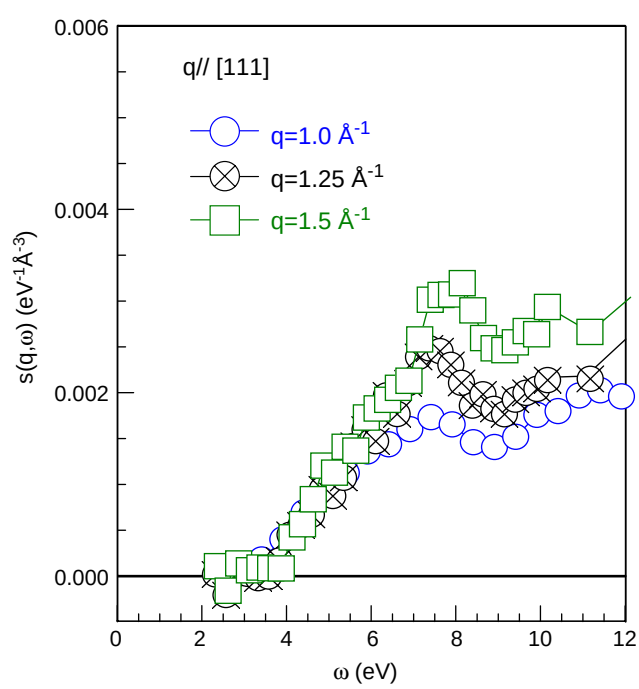

Fig. 2. IXS data for $s(\vec{q};\omega)$ for three wave vectors directed along the [111] direction.

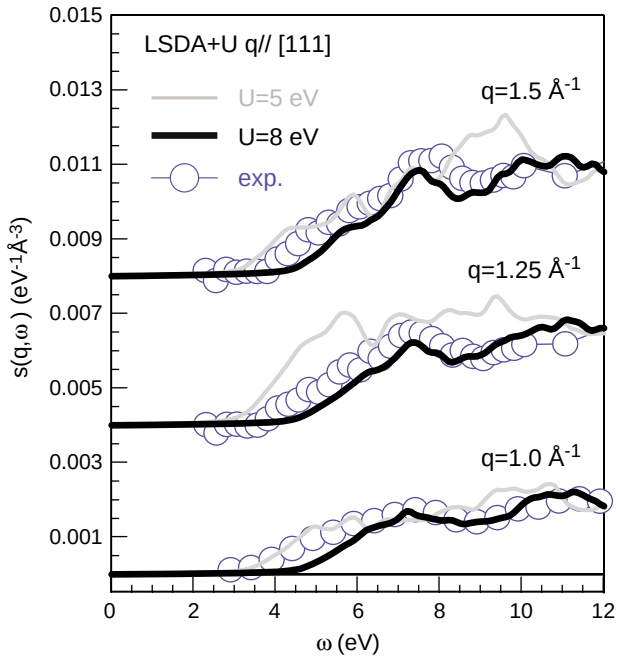

Fig. 3. Comparison between calculated $s(\vec{q};\omega)$ and the IXS data of Fig. 2. The spectra calculated on the basis of the LSDA+U ground state for $U=8$ eV (a value consistent with constrained LSDA calculations [15]) accounts extremely well for the main loss feature, lying at ~7.5 eV, for all three wave vectors.

shown in Fig. 2), the loss is not observed for small qs, and is diminished for qs larger than about 2 Å^{-1}.

The central issue contained in Fig. 3 is that the $s(\vec{q};\omega)$ calculated within LSDA+U/RPA for $U=8$ eV reproduces the IXS data faithfully, for all three wave vectors. We will argue, on the basis of Figs. 4–8, that this agreement is rooted on the physics of the 7.5 eV excitation, i.e., the agreement is not 'accidental.' This will allow us to conclude that the experimental data of Fig. 2 measure (indirectly) the LSDA+U electronic structure of Fig. 4 which corresponds to $U=8$ eV. (Consistent with this, it is self-suggestive that the LSDA+U/RPA spectrum obtained in Fig. 3 for $U=5$ eV, a value which we consider in this paper for illustrative/pedagogical purposes, clearly mis-represents the physics contained in the data of Fig. 2.)

In Fig. 4, we display what turns out to be the key subset of the electronic structure of NiO which is at stake in the present argument. The same refers to minority e_g states, for which the left panel shows the density of states (DOS), and the right panel shows the joint density of states (JDOS). The fact that the minority states are favored in this argument in place of the majority states is traced to the fact that the former provides a more abundant supply of empty states. Incidentally, note that this statement illustrates the fact that our investigation probes the empty states on the same footing with the occupied states, thus providing a 'one shot' investigation of the whole correlated-band structure in the vicinity of the optical gap.

Fig. 5 shows the dielectric function of NiO for one of the qs relevant in Fig. 2 (actually, the figure displays the $\vec{G}=0$, $\vec{G}'=0$ element of the dielectric matrix; the same contains the main physics, in the present case). The feature, which dominates the physics contained in Fig. 5 for q along [111] is the sizeable hump (structured peak) in Im ε. *It is important to notice that the same correlates well with the corresponding e_g–e_g feature in the JDOS (Fig. 4) which is obtained for $U=8$ eV.* (Note that this is consistent with the statement made in the previous paragraph about the subset of the electronic structure shown in Fig. 4 providing the crucial electron–hole channels.) Now an Im ε with this lineshape determines, by the structure of the Kramers–Kronig relation, a Re ε whose energy dependence is dominated by the pronounced 'wiggle' observed in Fig. 5 —and this wiggle *occurs in the energy interval relevant in Fig. 2*.

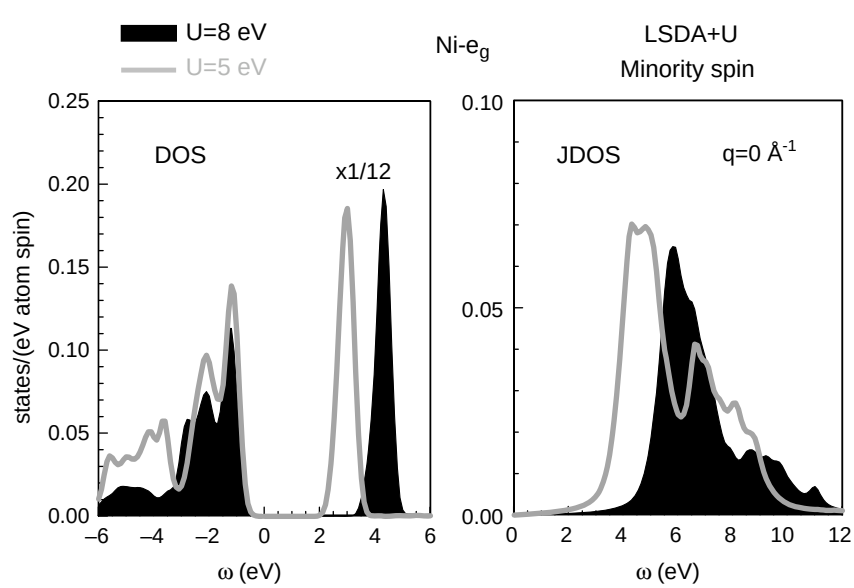

Fig. 4. LSDA+U-calculated DOS (left panel) and JDOS (right panel) for the minority Ni-derived e_g states. Results are presented for $U=8$ and 5 eV. As argued in the text, these states provide the crucial electron–hole channels from which the 7.5 eV loss feature of Fig. 2 originates. The IXS data of Fig. 2 is consistent with the electronic structure corresponding to $U=8$ eV.

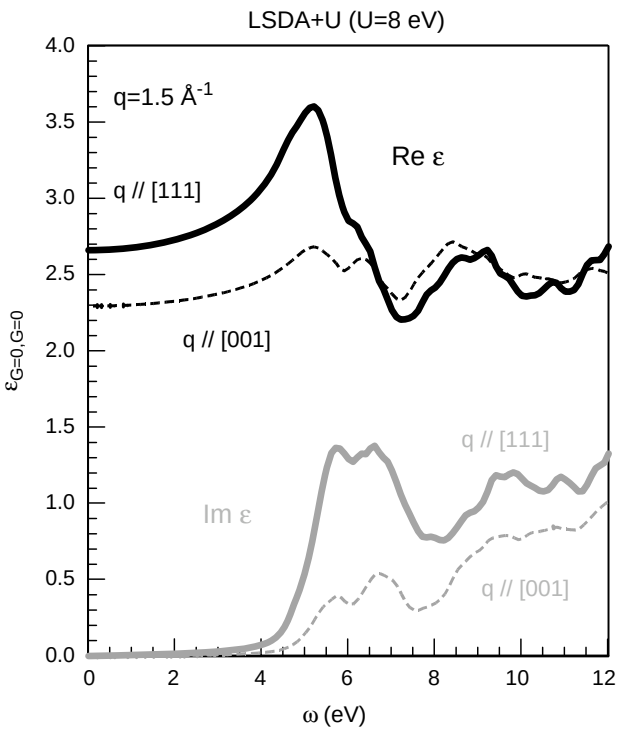

Fig. 5. Dielectric function of NiO calculated on the basis of the LSDA+U band structure (and in RPA) for $U=8$ eV. See text for details.

A dielectric function with a lineshape as that of Fig. 5 is known to be a good candidate for bringing about a well-defined peak in the inverse dielectric function [18]—without the need for the existence of an actual zero in Re ε. Since the inverse dielectric function is proportional to Im χ, such peak (if it is realized) translates into a loss peak in $s(\vec{q};\omega)$, according to Eq. (9). This is precisely what comes out of the full LSDA+U/RPA calculations (via Eq. (5)), as seen in Fig. 3, in excellent agreement with the IXS data of *Fig. 2*. *Thus, the contribution from the e_g–e_g electron–hole 'channels' of Fig. 4 to the*

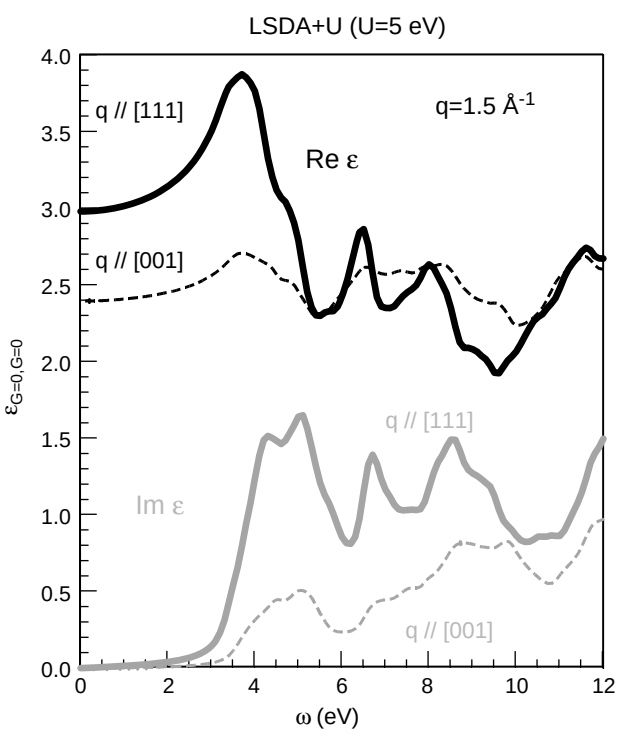

Fig. 6. Dielectric function of NiO calculated on the basis of the LSDA+U band structure (and in RPA) for $U=5$ eV. See text for details.

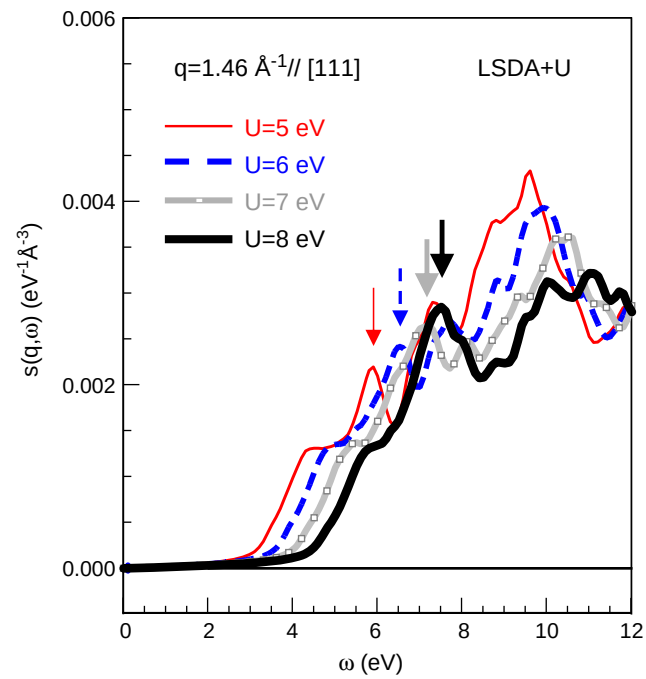

Fig. 7. Illustration of the dependence of the calculated energy position of the main above-gap loss feature for $q=1.46$ Å^{-1}, and directed along [111], on the value of U chosen in the underlying LSDA+U ground state.

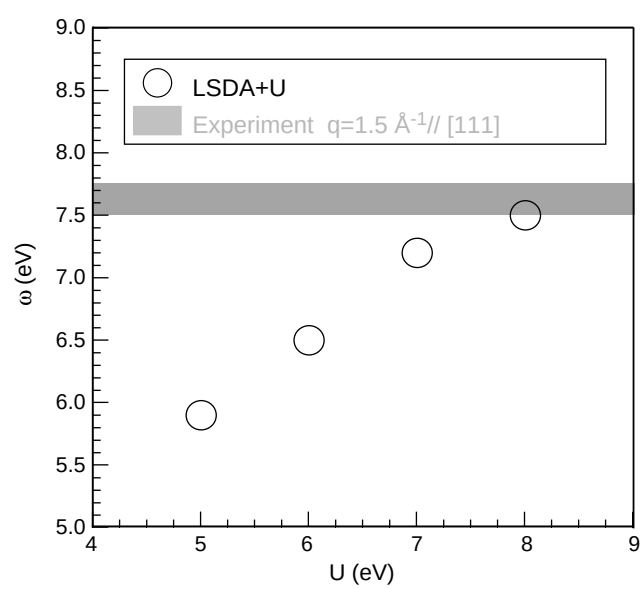

Fig. 8. Same as Fig. 7; here we record the calculated peak position vs. U together with the energetic position of the IXS peak ($\sim$7.5 eV). The fact that the peak position calculated for $U=8$ eV agrees with experiment, coupled with the 'collective' nature of the loss (see text) and in view of the apparent absence of strong beyond-RPA features in the data of Fig. 2, leads us to conclude that the IXS data discriminates in favor of the electronic structure shown in Fig. 4 for $U=8$ eV.

response function induces the formation of a collective mode, whose energy happens to be ~7.5 eV!

Significantly, as is observed in Fig. 6, the dielectric function which obtains for $U=5$ eV has the e_g–e_g peak in the 'wrong energy', i.e., it lies too low (*we are still referring to qs directed along [111]; we will discuss propagation along [001] below*). This leads to a collective mode in $s(\vec{q};\omega)$ lying at ~6 eV, which is clearly in disagreement with experiment (Fig. 3). Moreover, the additional fine structure in the Im ε of Fig. 6 is spurious, as is also concluded from Fig. 3. This fine structure is traced directly to the enhanced structure in the DOS for the occupied e_g states of Fig. 4 (this enhancement is relative to the electronic structure for $U=8$ eV). *Thus, the IXS data of Fig. 2 act as a sensitive arbiter of the quality of the electronic structure of Fig. 4*. The verdict is that the IXS data support the LSDA+U electronic structure which obtains for $U=8$ eV.

This message is further illustrated in Figs. 7 and 8. In the former, we show the $s(\vec{q};\omega)$ calculated for several values of U in the neighborhood of the value suggested by constrained LSDA calculations, $U=8$ eV. It is apparent that the energy location of the 'collective' feature is quite sensitive to the underlying choice of U and the ensuing electronic structure—*which as our analysis shows, manifests itself 'cleanly' via the* $s(\vec{q};\omega)$ *it generates.* This conclusion is further emphasized by the results of Fig. 8.

It should be borne in mind that the above conclusions were reached within our RPA description of the electron dynamics. We submit that the same is expected to be reliable, given the (apparent) absence of strong many-body (beyond-RPA) features in the IXS data of Fig. 2 (these effects would include, e.g., strong modification of the lineshape near the gap, which could be imputed to the many-body kernel f_{xc}).

Now the success of the LSDA+U functional reported thus far notwithstanding, additional results, contained in Figs. 9 and 10 suggest that the LSDA+U/RPA response method does not represent a complete theory.

Let us consider Fig. 9 first. In it we show IXS data for $s(\vec{q};\omega)$ corresponding to three wave vector transfers directed along the [001] direction, together with the results of LSDA+U/RPA calculations. It is apparent that the spectra calculated for $U=8$ eV do not do as well as they did in Fig. 3. We interpret this situation as follows. The reason that $U=8$ eV turned out to work in Fig. 3 is that *in that case the loss spectra are controlled by the collective mode at 7.5 eV, whose physics is in turn controlled by the "global" energy location of the* e_g–e_g *electron–hole channels displayed in Fig. 4*. As discussed above, the LSDA+U functional for $U=8$ eV happens to place these excitation channels in the correct energy location, *as monitored by the IXS data* (more conventionally, this would be argued on the basis of photoemission and inverse-photoemission measurements [10]). By contrast, the loss spectra for qs along [001] are controlled by fine structure in the correlated band structure, and the same is hard to reproduce on the basis of a one parameter functional.

One may still ask why it is that LSDA+U/RPA theory for $U=8$ eV yields a collective mode for qs along [001], while the same is not present in the IXS data in Fig. 9 (this discrepancy is

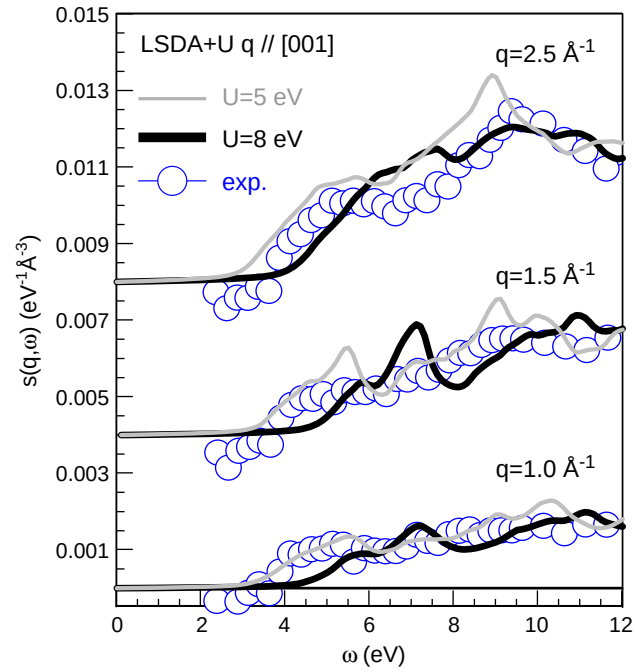

Fig. 9. Comparison between calculated and measured $s(\vec{q};\omega)$ for wave vector transfers directed along [001]. Note that the IXS data does not feature the 7.5 eV loss which dominates the data for [111] (Fig. 2). See text.

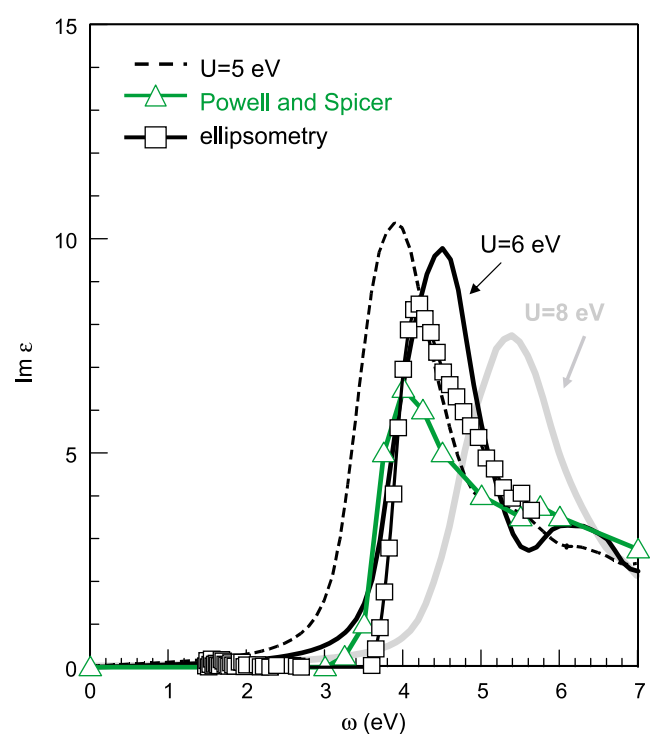

Fig. 10. Comparison between the calculated (in RPA) dielectric function of NiO, in the optical limit, with our ellipsometry data; for completeness, the reflectivity-derived data of Ref. [36] is also shown. This figure (as Fig. 7, in the case of IXS data) illustrates the dependence of the LSDA+U-based result on the choice of U. See discussion in text.

most evident in the spectrum for $q = 1.5$ Å^{-1}). We believe that the answer is as follows. As Fig. 5 makes clear, the *matrix elements* which control how the JDOS (which 'measures' exclusively the availability of electron–hole channels) 'propagates' into Im ε, *clearly enhance the actual e_g–e_g excitation process, for qs along [111], vs. qs along [001]. This trend is clearly in agreement with the experiment—it is consistent with the nature of the IXS data in Figs. 3 and 9. In fact, this enhancement is behind the success story of RPA dynamics we have for qs along [111].* (Ultimately, this behavior of the matrix elements is determined by overlaps between the lobes for e_g electron and hole orbitals.) Unfortunately, the matrix elements do not suppress completely the 'remnant,' weak e_g–e_g modulations in Im ε for qs along [001]; the upshot is that in the RPA these weak transitions still manage to yield the loss peak present in the calculated $s(\vec{q};\omega)$ of Fig. 9. We stress that actual calculation shows that the strength of the calculated loss in Fig. 9 is significantly enhanced by the crystal local fields (matrix nature of χ_s); thus, the full analysis is not trivial.

Now, since the underlying electronic structure for $U = 8$ eV has already been validated by our previous discussion, we submit that beyond-RPA effects, which in our TDDFT-like picture will be introduced by f_{xc}, must be important in the case of Fig. 9 (presumably, for $U = 8$ eV); in other words, such many-body effects should 'erase' the impact on the $s(\vec{q};\omega)$ of Fig. 9 of the weak structure in Im ε for q along [001] (Fig. 6). *This would not be too surprising, as these 'excitonic' effects are known to compete with the crystal local fields[33,34].*

Consider, finally, Fig. 10, which refers to the optical limit [35]. First of all, we note that the dielectric functions obtained from our ellipsometry measurements deviate rather markedly from the dielectric functions of Powell and Spicer [36], which were obtained by Kramers–Kronig analysis of normal-incidence reflectivity measurements. Discrepancies between (more accurate) ellipsometry-derived measurements and reflectivity-derived dielectric function measurements are not unusual. These discrepancies result from the fact that in ellipsometry, Re ε and Im ε are obtained directly from the measurement of parameters, while normal-incidence reflectivity dielectric function measurements involve Kramers–Kronig integration with extrapolations to zero energy and to infinite energy to obtain convergence. Going back to the performance of theory, what stands out in Fig. 10 is how poorly the spectrum calculated for the 'ab initio' value [15] of the on-site interaction, $U = 8$ eV, does.

In fact, and for the sake of the present discussion, we note that the LSDA + U/RPA optical spectrum would appear to be 'optimal' for $U = 6$ eV. But, as spelled out at the outset, here we are not advocating using the results of Fig. 10—and the previously discussed IXS data as well—to 'pin down' a 'physical' value of U. On the contrary, the ellipsometry data, in conjunction with the IXS data, highlight the limitations of a response framework, the LSDA + U/RPA, in which the strong atomic-like correlations are controlled by a single parameter (the Hubbard U).

At this point, it may be useful to note that this situation is similar to the well-known example of the photoemission spectrum of Ni [37]. In that problem, the simple Hubbard model is able to account for the existence of the 6 eV satellite peak—a hallmark of strong hole–hole correlations—and for the reduction in the exchange splitting (relative to single-particle theory). However, if the value of the Hubbard U is chosen in such a way that the theory reproduces the satellite structure, the description of the splitting worsens—and vice versa [37].

Moreover, accepting our premise (put forth earlier in this paper) that it is meaningful (at least qualitatively) to reason à la TDDFT, it is entirely possible that a numerical exercise such as the one illustrated in Fig. 8 is not very consequential. Indeed, it is likely that such comparison is hiding the effects of bona fide dynamical correlations, due, e.g. to the electron–hole attraction. A full assessment of the performance of the LSDA + U functional is thus expected to require the inclusion of such physics, which would introduce the U into a non-trivial f_{xc}. This is why we do not subscribe to the strategy of papers such as Ref. [14], which concluded that on the basis of the reflectivity data of Ref. [36], one could adopt the value $U = 5$ eV for optics. Interestingly, such conclusion has been endorsed in Ref. [38], which sends the message that the same is sound. By contrast, and to reiterate, from Fig. 10 (and earlier, from Fig. 9, which covers a larger phase space) we submit that LSDA + U/RPA theory is not a complete theory; the role of U in the dynamics must be included before we can engage in general recommendations as to what value of U may work 'universally' (i.e., for the whole phase space) for a given material—and, as noted above, a single parameter theory may not be enough, for the entire electron–hole phase space.

This conclusion is not contradictory with our conclusion drawn earlier, on the basis of the IXS data of Fig. 2, namely, that the IXS data supported the $U = 8$ eV electronic structure depicted in Fig. 4. As argued at length on the basis of Figs. 4–8, the signature of the electronic structure of Fig. 4 built into Fig. 2 arises via the collective excitation featured in the IXS data. That physics is not present in, e.g., the optical data.

In summary, the $s(\vec{q};\omega)$ predicted on the basis of the LSDA + U/RPA method, for the constrained-LSDA value of U ($U = 8$ eV) is in excellent agreement with the IXS data of Fig. 2. Moreover, because of the collective nature of the measured loss, and the fact that the same provides a direct mapping of the electronic structure depicted in Fig. 4 for $U = 8$ eV, we conclude that the IXS data of Fig. 2 discriminate in favor of the corresponding electronic structure. We also stress that this result illustrates the merit of IXS, in combination with correlated-band-structure theory, for the investigation of the electronic structure of strongly correlated materials. A complete theory would need to go beyond LSDA + U/RPA in several directions; most importantly, we have argued that beyond-RPA effects are likely to play a significant role in Figs. 9 and 10.

Acknowledgements

A.G.E. acknowledges support from NSF ITR DMR-0219332. Research at ORNL is sponsored by the DOE, Office

of Science, DMS under contract with UT-Battelle, LLC. The UNICAT beamline is supported by the FS-MRL, ORNL, NIST, and UOP Res, LTD. The Advanced Photon Source is supported by the DOE.

References

[1] P. Hohenberg, W. Kohn, Phys. Rev. 136 (1964) B864.

[2] W. Kohn, L.J. Sham, Phys. Rev. 140 (1965) A1133.

[3] For reviews of density-functional theory see, e.g.,S.B. Trickey (Ed.), Density Functional Theory of Many–Fermion Systems, Academic, NY, 1990; R.M. Dreizler, E.K.U. Gross, Density Functional Theory: An Approach to the Quantum Many-Body Problem, Springer-Verlag, Berlin, 1990; R.O. Jones, O. Gunnarsson, Rev. Mod. Phys., 64 (1989) 689.

[4] J. Perdew, A. Zunger, Phys. Rev. B 23 (1981) 5048.

[5] W.M. Temmerman, A. Svane, Z. Szotek, H. Winter, in: J.F. Dobson, G. Vignale, M.P. Das (Eds.), Electronic Density Functional Theory: Recent Progress and New Directions, Plenum Press, New York, 1998, p. 327.

[6] V.I. Anisimov, J. Zaanen, O.K. Andersen, Phys. Rev. B 44 (1991) 943.

[7] V.I. Anisimov, I.V. Solovyev, M.A. Korotin, M.T. Czyzyk, G.A. Sawatzky, Phys. Rev. B 48 (1993) 16929.

[8] A.I. Liechtenstein, V.I. Anisimov, J. Zaanen, Phys. Rev. B 52 (1995) R5467.

[9] A.B. Shick, A.I. Liechtenstein, W.E. Pickett, Phys. Rev. B 60 (1999) 10763.

[10] For a review of the LDA+U method, see V.I. Anisimov, F. Aryasetiawan, O. Gunnarsson, J. Phys.: Condens. Matter 9 (1997) 767.

[11] Implementations of the LSDA+U method are now available in general-purpose codes, such as the WIEN2k package, which we use in the present work (Ref. [25]).

[12] E. Runge, E.K.U. Gross, Phys. Rev. Lett. 52 (1984) 997.

[13] For reviews of TDDFT see E.K.U. Gross, J.F. Dobson, M. Petersilka, in: R.F. Nalewajski (Ed.), Density Functional Theory II, Springer, Berlin, 1996, p. 81; K. Burke, E.K.U. Gross, in: D. Joubert (Ed.), Density Functionals: Theory and Applications, Springer, Berlin, 1998, p. 116.

[14] O. Bengone, M. Alouani, P. Blöchl, J. Hugel, Phys. Rev. B 62 (2000) 16392.

[15] M.S. Hybertsen, M. Schlüter, N.E. Christensen, Phys. Rev. B 39 (1989) 9028; I.V. Solovyev, P.H. Dederichs, Phys. Rev. B 49 (1994) 6736.

[16] S.L. Dudarev, G.A. Bottom, S.Y. Savrasov, C.J. Humphreys, A.P. Sutton, Phys. Rev. B 57 (1998) 1505.

[17] K.-W. Lee , J. Kuneš, W. E. Pickett, cond-mat/0403018.

[18] For a recent review of IXS, see W. Schülke, J. Phys.: Condens. Matter 13 (2001) 7557.

[19] In our case, the electrons interact with the hard X-rays coming out of the synchrotron via the A^z term in the electron–photon interaction, A being the vector potential. Standard quantum-mechanical manipulations show that the relevant response function is precisely that defined by Eq(4), obeying Eq (5).

[20] This non-trivial conclusion is behind the physical outlook we adopt, when we graft the TDDFT method into a response calculation relying on the use of the ground state provided by the LDA+U method, which is not quite a Kohn-Sham method.

[21] M. Petersilka, U.J. Gossmann, E.K.U. Gross, Phys. Rev. Lett. 76 (1996) 1212.

[22] W. Ku, A.G. Eguiluz, Phys. Rev. Lett. 82 (1999) 2350.

[23] W. Ku, W.E. Pickett, R.T. Scalettar, A.G. Eguiluz, Phys. Rev. Lett. 88 (2002) 057001.

[24] I.G. Gurtubay, W. Ku, J.M. Pitarke, A.G. Eguiluz, B.C. Larson, J. Tischler, P. Zschack, Phys. Rev. B 70 (2004) 201201(R).

[25] P. Blaha, K. Schwarz, G.K.H. Madsen, D. Kvasnicka, J. Luitz, WIEN2k, An Augmented Plane Wave + Local Orbitals Program for Calculating Crystal Properties, Karlheinz Schwarz, Techn. Universität Wien, Austria, 2001, ISBN: 3-9501031-1-2.

[26] T. Grabo, T. Kreibich, S. Kurth, E.K.U. Gross, in: V. Anisimov (Ed.), Strong Correlations in Electronic Structure: Beyond the Local Density Approximation, Gordon and Breach, 1999; M. Petersilka, U.J. Gossmann, E.K.U. Gross, in: J.F. Dobson, G. Vignale, M.P. Das (Eds.), Electronic Density Functional Theory: Recent Progress and New Directions, Plenum Press, New York, 1997, p. 177.

[27] The numerical convergence has been checked by performing calculations with 8x8x8, 12x12x12 and 14x14x14 k-meshes without observing appreciable changes in the spectra. Most of the results described herein have been obtained using a 12x12x12 k-mesh, with 189 k-points in the irreducible wedge of the Brillouin zone. For completeness, other numerical parameters entering our computations are as follow: The broadening parameter in the energy-denominator entering the Kohn-Sham response χ_s was taken to be 0.2 eV. The number of bands kept in the calculation of χ_s is typically 76 (counting the semicore states), which corresponds to keeping empty bands up to 70 eV above the gap; with this cut-off, our spectra are well converged for all energies relevant in this paper.

[28] J.Z. Tischler, B.C. Larson, P. Zschack, A. Fleszar, E.G. Eguiluz, Phys. Stat. Sol. (b) 237 (2003) 280.

[29] G.E. Jellison Jr., F.A. Modine, Two-modulator generalized ellipsometry: experiment and calibration, Appl. Opt. 36 (1997) 8184–8189; G.E. Jellison Jr., F.A. Modine, Two-modulator generalized ellipsometry: theory, Appl. Opt. 36 (1997) 8190–8198.

[30] D.A.G. Bruggeman, Ann. Phys. 24 (1935) 636 Leipzig.

[31] G.E. Jellison Jr., Thin Solid Films 313–314 (1998) 33–39.

[32] For the anti-ferromagnetic ground state of NiO, the Kohn-Sham density response χ_s contains separate contributions from minority (χ_s^{min}) and majority (χ_s^{maj}) spin states. The demonstration that Eq. (5) holds in RPA, with $\chi_s = \chi_s^{min} + \chi_s^{maj}$ is elementary.

[33] W. Hanke, L.J. Sham, Phys. Rev. B 21 (1980) 4656.

[34] G. Onida, L. Reining, A. Rubio, Rev. Mod. Phys. 74 (2002) 601.

[35] Strictly, the optical limit corresponds to $q=0$, which our calculations simulate accurately enough via the evaluation of the dielectric function for a small-enough wave vector; the figure refers to $|q|=0.16$ Å^{-1}; several tests indicate that the optical spectrum is converged sufficiently well.

[36] R.J. Powell, W.E. Spicer, Phys. Rev. B 2 (1970) 2182.

[37] A. Liebsch, Phys. Rev. B 23 (1981) 5203.

[38] A.G. Petukhov, I.I. Mazin, L. Chioncel, A.I. Liechtenstein, Phys. Rev. B 67 (2003) 153106.